THE ASTROPHYSICAL JOURNAL, 408:428–445, 1993 May 10

FLOW DYNAMICS AND BENDING OF WIDE-ANGLE TAILED RADIO SOURCES

AILEEN A. O'DONOGHUE
National Radio Astronomy Observatory[1], Physics Department and Astrophysics Research Center, New Mexico Institute of Mining and Technology; and Physics Department, St. Lawrence University, Canton, NY 13617
JEAN A. EILEK
Physics Department and Astrophysics Research Center, New Mexico Institute of Mining and Technology, Socorro, NM 87801
AND
FRAZER N. OWEN
National Radio Astronomy Observatory[1], P.O. Box O, Socorro, NM 87801
Received 1991 May 13; accepted 1992 September 8

ABSTRACT

VLA observations of 11 wide-angle tailed radio sources (WATs) at 6 and 20 cm are used to study the dynamics of this class of source. These new images, in conjunction with optical and X-ray data, are used to describe the unifying characteristics of this class. WATs are found in the centers of clusters without cooling cores, associated with galaxies of low space velocity. They are large sources, extending at least 50 kpc from the cluster center, and they have radio power close to the Fanaroff-Riley (F-R) I/II break. They show a distinctive jet-hot spot transition which is not seen in either F-R type II sources, or in lower power F-R type I sources. The bend into the characteristic C shape occurs at the hot spots.

We use the surface brightness and spectral distributions to model the flow fields and bending dynamics of the sources. We use two limiting models, the adiabatic model (in which no in situ energization takes place), and the kinetic model (in which all of the radio luminosity comes from in situ energization). We find the sources cannot be bent by the slow galaxy motion in the kinetic model. We find the sources can be bent by the ram pressure of a slowly moving central galaxy in the adiabatic model. However, this model has serious problems reconciling the particle lifetime and the travel time down the tail.

Subject headings: galaxies: jets — galaxies: kinematics and dynamics — galaxies: photometry

1. INTRODUCTION

Wide-angle tailed radio sources (WATs) were first defined by Owen & Rudnick (1976). The defining criteria they put forth are (1) C-shaped radio emission for bent sources at low resolution, (2) association with Owen & Rudnick (1976) optical type 1 cluster galaxies that are single, cluster-dominant galaxies, and (3) intermediate radio luminosity (10^{42} ergs^{-1} < L_{WAT} < 10^{43} ergs s^{-1}). Their radio luminosity is comparable to that of the Fanaroff-Riley (1974) break between their type I sources (lower power, tailed radio morphology) and their type II sources (higher power, classical double morphology), namely, 2×10^{25} W Hz^{-1}, converted to 1400 MHz assuming a spectral index of 0.7. These sources tend to be more powerful than the narrow-angle tailed sources (NATs) studied by O'Dea (1984); and, unlike the NATs, the jets in WATs are generally straight (except for local wiggles or kinks) until they disrupt into hot spots and tails.

X-ray emission from nearby clusters of galaxies containing WATs shows that these sources sit in an atmosphere of hot, thermal gas. The clusters in which WATs are found do not exhibit the centrally peaked X-ray emission characteristic of cooling flows (Norman, Burns & Sulkanen 1988). Radio sources associated with central galaxies in cooling cores seem to be different from the WATs; they are smaller, lower in radio power and may have different morphologies (e.g., O'Dea & Baum 1986; Ge 1991; Zhao 1990). The gas in the central regions of clusters of galaxies without cooling cores is typically at a temperature $T \sim 5 \times 10^7$ K, and a density $n_{ICM} \sim 10^{-3}$ cm^{-3} (Jones & Forman, 1984). Only three of our sources sit in clusters for which we know of X-ray data: Abell 98, Abell 160 (Feretti et al. 1990) and Abell 1446 (Burns & Balonek 1982). In addition, X-ray data exist for two other clusters containing well-studied WATs: Abell 400 (containing 3C 75; Caganoff, Bicknell, & Carter 1985) and Abell 2634 (3C 465; Eilek et al. 1984). The density and temperature we assume, above, does describe the X-ray emitting gas in these clusters. We will therefore assume that all of our sources sit in such a hot, thermal atmosphere. Velocity dispersion studies of clusters containing cD galaxies found that these galaxies, which include the parent galaxies of WATs, are moving at only a few hundred kilometers per second with respect to the mean velocity of the cluster galaxies. Quintana & Lawrie (1982), using published work up to that date, find a mean velocity ~300 km s^{-1} for 20 central dominant galaxies relative to the cluster mean. Two of the largest cD velocities relative to the cluster mean are those of the central galaxy in Abell 1795 (~370 km s^{-1} relative to the cluster mean; Hill et al. 1988), and that in Abell 2670 (~440 km s^{-1}; Sharples, Ellis & Gray 1988). Thse are unusually large velocities for central dominant galaxies. Simulations of cD galaxy formation during the evolution of a rich cluster, by Malumuth (1989), predict the velocity of the galaxy relative to the cluster mean to be $\lesssim$200 km s^{-1} in nearly all cases.

The initial point of interest in these sources was the mechanism for bending them into the observed C shapes. Owen & Rudnick (1976) anticipated that the bending would be simply explained by the motion of the galaxy through the intracluster medium (ICM). The bending of NATs does seem to be

[1] Operated by Associated Universities, Inc., under cooperative agreement with the National Science Foundation.

explained in this way (Jones & Owen 1979; O'Dea 1984). However, when the low velocities of the parent galaxies of WATs, relative to the ICM, were taken into account (Eilek et al. 1984), it turned out the bending of the WATs studied in detail could not be explained. In this paper we extend the study of bending to a larger set of sources.

A set of 11 wide-angle tailed radio sources (WATs) was observed with the VLA from 1984 to 1986. The images and details of the observations are presented in O'Donoghue, Owen, & Eilek (1989); hereafter O^2E). The observations were intended to expand the data base of WATs, allowing examination of the class definitions put forth by Owen & Rudnick (1976), separation of class and source characteristics, and investigation of the flow dynamics as applied to the problem of bending these sources (Burns 1981; Eilek et al. 1984; Leahy 1984). The sources were chosen from a 1400 MHz survey of Abell clusters (Owen et al. 1982) and subsequent VLA observations (Owen, White, & Burns 1991). They were picked on the basis of their flux density ($\gtrsim$ a few hundred mJy), their angular size ($\gtrsim 1$), their redshift ($z \lesssim 0.1$) and their general WAT-like appearance in low-resolution images. However, a variety of morphologies was chosen in an attempt to sample the fringes of the class.

In the first section of this paper we present a synthesis of the data presented in O^2E. The class parameters are examined through comparisons of radio luminosities and morphologies as well as the optical magnitude and cluster membership of the parent galaxies.

The bulk of the paper is an examination of the flow dynamics and the problem of bending WATs. The bending problem must be studied in the context of the dynamics of the sources. Assumptions about the nature of the flow must be made in any attempt to explain the bending. The current literature assumes that radio sources are hydrodynamic phenomena, with the mass and energy in the extended lobes being supplied by a continuous flow from the nucleus. There is a general assumption that the F-R type II sources involve supersonic flow (e.g., the simulations of Norman et al. 1982), while F-R type I sources are subsonic flows (e.g., Bicknell 1984, 1986a, b, c). Within this context, two types of models have arisen to address the surface brightness and dynamics of tailed radio sources (the F-R type I's). The first of the models we call the adiabatic model (introduced by Fanti et al. 1982), in which the relativistic particles observed by their radio luminosity are given the energy necessary to shine in the core or engine of the source. There is no acceleration of particles by any processes beyond the core. The surface brightness of the flow, in this model is accounted for by a mixture of jet deceleration and lateral expansion. The alternate theory we call the kinetic model (e.g., Jones & Owen 1979; Eilek et al. 1984), in which the particles are accelerated outside the core by fluid processes (shocks or turbulence) so that the total luminous energy observed must have been transported down the jet and tail as kinetic energy. Both models require that the flow decelerate as it goes away from the galaxy. The adiabatic model needs this to offset the expansion of the jet or tail, in order to maintain the surface brightness. The kinetic model needs this in order to create radio luminosity from the flow kinetic energy. While neither model has addressed the dynamics of why or how the flow decelerates, it is generally assumed that the flows are sub- or transonic and that they entrain ambient matter through turbulence. This entrainment must then decelerate the flow.

Bicknell (1984) considered an extension of the adiabatic model, which added turbulent entrainment of magnetic field and dissipation of turbulent energy through particle acceleration, to the basic Fanti et al. (1982) model. Bicknell's model thus blends our two models, which we consider as limiting but simple cases. We find in this paper that neither of these simple models, as we formulate them, can account for the bent WATs. We return to possible hybrid models, or other extensions of the basic picture, in the concluding discussion.

The rest of this paper is organized as follows. In § 2, we review the physical parameters of our sources and discuss the general properties we think are important in defining the class of WATs. In § 3, we present the two models, adiabatic and kinetic. We use each to derive the velocity fields in the tails, and we test the adiabatic model by evaluating particle lifetimes. In § 4 we use the velocity fields to test the ram pressure bending model. Finally, in § 5, we consider how the problems discovered in both the adiabatic and kinetic models might be alleviated by extending the theories. We relegate details of the physics, and of the models, to the Appendices.

2. WATs AS A CLASS

2.1. *Traditional Definition of WATs*

One goal of this project was to identify global characteristics that distinguish WATs from the variety of other extended extragalactic radio sources. Traditionally, WATs have been set apart from other radio sources by their C-shaped morphology and their association with dominant galaxies in the centers of clusters. Sources meeting these criteria also turned out to have radio powers close to the F-R break. The sources in O^2E can be evaluated with respect to these definitions and the definitions can, in turn, be evaluated in light of the new data.

To explore the limits of the class, a variety of morphologies was selected for the project. All the sources are displayed on the same scale in Figure 1, which is reproduced from O^2E. All of the sources show bright hot spots close to the core, and tails past the hot spots, which broaden and grow fainter in surface brightness, going away from the core. With one exception, the sources all show bends away from the initial jet direction, and all that bend do so into a C-shape. The angle by which each tail bends, relative to its jet, ranges from 30° to 115° (see Table 3 of O^2E). In general, the strongest bend occurs at the hot spot. Past their hot spot, the tails show substructure and some bending, but to a first approximation stay straight after their bend at the hot spot. The only source which is not at all bent or C-shaped is 0043+201. This could, of course, be a bent source seen in projection; it shares the other properties of the sample, and we consider it also a WAT.

The sources are listed in Table 1, where their important properties are summarized. The flux densities (at 20 cm) were taken from single dish observations done by Owen et al. (1982) and the redshifts from Owen, White, & Thronson (1988). These sources show a strikingly narrow range of monochromatic luminosities, ranging from 0.5×10^{25} W Hz^{-1} to 5×10^{25} W Hz^{-1}. These luminosities compare well with the original criterion of Owen & Rudnick (1976). All of our WATs are close to the F-R break 2×10^{25} W Hz^{-1} at 1400 MHz.

The parent galaxies tend to be in Bautz-Morgan type I or II clusters (Bautz & Morgan 1970) and lie between a projected distance of 0.02 and 0.3 of an Abell radius from the normal cluster center as estimated by Abell (1958) (see Table 1 of O^2E). The parent galaxies are among the largest and most luminous galaxies in the universe (Owen & Laing 1989; Owen & White

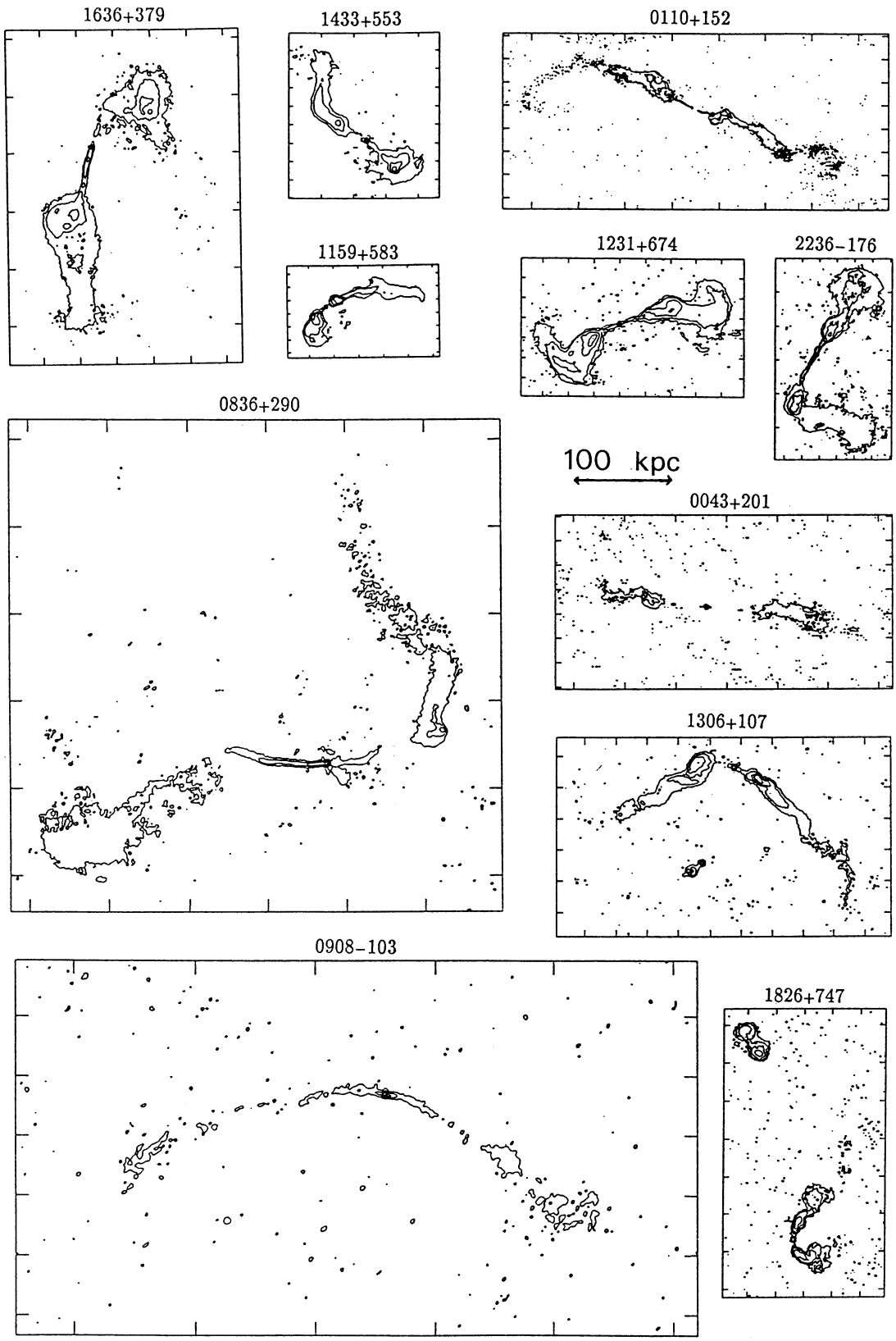

FIG. 1.—All the sources in the small survey of WATs are shown to the same linear scale

TABLE 1

THE SOURCES

Source	Abell Cluster	z[a]	Abs. Mag.[a]	B-M Class	Distance to Center[b]	S_{1400} (Jy)	Monochromatic luminosity (W Hz^{-1})	Total luminosity (ergs s^{-1})
0043+201	98	0.1063	−23.53	II-III[c]	0.08[d]	0.9	1.1×10^{25}	3.0×10^{42}
0110+152	160	0.0447	[e]	III[f]	0.09[d]	1.0	0.4×10^{25}	5.2×10^{41}
0836+290	690	0.0788	−23.78	I[g]	0.02[d]	0.8	1.1×10^{25}	1.5×10^{42}
0908+103	791	0.129	−23.75[h]	[e]	[e]	0.6	2.1×10^{25}	3.0×10^{42}
1159+583	1446	0.1018	−23.40	I[i] II-III[j]	0.07[d]	1.0	2.2×10^{25}	3.1×10^{42}
1231+674	1559	0.1062	−24.02	I[i]	0.07[d]	0.9	2.1×10^{25}	3.0×10^{42}
1306+107	1648	0.136	−24.11[h]	II[i]	0.30[d]	0.1	0.5×10^{25}	5.5×10^{41}
1433+553	1940	0.1396	−23.79	II[c,f]	0.07[k]	0.5	2.2×10^{25}	2.9×10^{42}
1636+379	2214	0.161	−23.53	II[l]	0.27[d]	0.6	3.6×10^{25}	4.6×10^{42}
1826+747	2306	0.121	−23.15[h]	II[l]	0.06[k]	0.6	1.9×10^{25}	2.6×10^{42}
2236−176	2462	0.0698	−23.54	II[j]	0.11[d]	1.7	1.7×10^{25}	2.4×10^{42}

[a] Owen, White, & Thronson 1988.
[b] Fraction of corrected Abell radius (see O^{2}E).
[c] Bautz 1972.
[d] Owen 1975.
[e] Not available.
[f] Bautz & Morgan 1970.
[g] Roland et al. 1975.
[h] Based on estimated redshift.
[i] McHardy 1974.
[j] Leir & van den Bergh 1977.
[k] Rudnick and Owen 1977.
[l] Simon 1978.

1991). This is particularly striking because they give rise to radio sources of only intermediate power.

2.2. *Source Features*

In this section we present the global properties of the sources, and consider what important properties of the sources have in common, that extend the definition of the class of WATs.

2.2.1. *Radio Cores and Jets*

All the sources exhibit unresolved radio cores. Their monochromatic luminosities at 1400 MHz are listed in Table 2.

Jets were detected in all the sources except 1826+747. Only a few of the jets exhibit any bends. Most notable are the sharp bends in the southern jet of 1231+674. Although these jets are notably brighter at the bends, no general trend of brightening at, before, or after the bends in the jets is observed in the survey.

We summarize the jet properties in Table 2. The jet properties were measured at several (typically ~5) positions along the jet (shown in O^{2}E); we present mean values here. In Table 2 we show the monochromatic luminosity from each jet, the sidedness ratios, the jet radii, and the minimum pressure. The monochromatic luminosity is the mean of the two jets for each

TABLE 2

JETS AND CORES

Source	Core Power (W Hz^{-1})	Jet Power (W Hz^{-1})	Sidedness	Jet Radius (kpc)	Jet p_{min} (dyn cm^{-2})
0043+201	2.2×10^{23}	9.4×10^{22}	1.5	0.5[a]	6.1×10^{-12}
0110+152	2.1×10^{22}	4.5×10^{22}	1.6	0.4[a]	2.0×10^{-11}
0836+290	1.3×10^{24}	1.8×10^{24}	2.3	1.9	4.9×10^{-12}
0908−103[b]	2.0×10^{23}	...	...	...	...
1159+583	1.2×10^{23}	6.6×10^{23}	15.8[c]	0.9	3.0×10^{-11}
1231+674	1.3×10^{23}	2.8×10^{23}	1.8	0.9	1.9×10^{-11}
1306+107	2.5×10^{23}	1.7×10^{23}	2.8[c]	2.0[a]	4.1×10^{-12}
1433+553	5.2×10^{23}	2.8×10^{23}	3.2	1.9[a]	1.1×10^{-11}
1636+379	2.5×10^{23}	3.3×10^{23}	10	1.3[a]	3.9×10^{-11}
1826+747[d]	1.3×10^{23}	...	...	...	...
2236−176	9.4×10^{22}	2.2×10^{24}	4.1	0.88	4.2×10^{-11}

[a] Significant portion (>20%) of jet unresolved.
[b] No jet definable; consists of flaring tails.
[c] Lower limit; one side undetected.
[d] No jet detected.

source; the remaining three quantities are means of the measurements along both of the jets. Thirteen of the jets are only partly resolved at 20 cm; in these cases, we use half of the beamwidth as an upper limit to the radius. We find that the jet luminosity is uniformly less than the core luminosity at 20 cm, and no trend of $P_{\rm core}$ relative to $P_{\rm jet}$ is apparent. This result differs from that of Burns et al. (1984), who noted a possible trend, $P_{\rm core} \propto P_{\rm jet}$ at 6 cm, for a data set including some F-R II sources with detected jets and some F-R I sources. The numbers in Table 2 indicate that the jets have internal pressures similar to, or slightly less than that of the ambient medium ($P_{\rm ICM} \sim 10^{-11}$ dyn cm^{-2}, from the density and temperature given above.) For the jets which are not fully resolved, these values are only lower limits to $P_{\rm min}$.

The sidedness of the jets—the side-to-side ratio of their luminosity—ranges from the equal (in length and surface brightness) jets of 0043+201 to the more than one to 10 sided jets of 1159+583. We used the sidedness of the jets to determine a limit on the flow velocity in light of relativistic beaming. The surface brightness ratios in Table 2 can be interpreted in the light of Monte Carlo simulations done by O'Dea (1984). The Doppler enhancement of two beams of velocity $\beta = v/c$ and inclination angle to the line of sight θ is

$$\frac{S_1}{S_2} = \frac{(1 - \beta_2 \cos \theta_2)^{(2+\alpha)}}{(1 - \beta_1 \cos \theta_1)^{(2+\alpha)}}, \quad (1)$$

where $\alpha = -d \ln S(\nu)/d \ln \nu$ is the usual spectral index. O'Dea studied the intensity ratios for a random distribution of inclinations of 10^4 sources taking $\beta_1 = \beta_2$ and $\theta_1 = \theta_2 - \pi$ and the power spectrum spectral index as $\alpha = 0.65$. He found that $\beta = 0.2$ produced an intensity ratio ranging from 2 to 3. The data presented in Table 2 indicate that, with the notable exceptions of 1159+583, 1636+379, and 2236−176, the surface brightness ratios are close to this range. Thus, the initial jet velocity in these galaxies is unlikely to be greater than $0.2c$; we will use this in the analysis below.

2.2.2. *Hot Spots*

Most of the sources have hot spots detected near the core, and the surface brightness of the tails falls off with distance from the core, in agreement with the general F-R I morphology. The transition from the jet to the hot spot is usually dramatic, in that the source makes a sudden transition from a faint, narrow jet to a brighter and broader region, which we call a hot spot. In several of our images the jet can be followed within the hot spot. Past the hot spot the source continues into a broad tail. This sudden jet/hot spot transition is also seen in other well-studied WATs (e.g., 3C 465, Eilek et al. 1984; 1919+479, Burns 1981; to a lesser extent in 3C 75, Owen et al. 1985); it seems to be characteristic of the class.

We summarize hot spot properties in Table 3. We list the ratio of the mean jet surface brightness to the peak hot spot surface brightness; the typical brightening is a factor of 2.5 in flux density. We show the distance of the hot spots from the core; most hot spots are at several tens of kiloparsecs from the core. Gaussian fits to slices across the hot spots allow rather uniform estimation of their sizes (the Gaussian halfwidth of the fit). We give the expansion factor (hot spot size to jet size); the flow expands by a factor of 3–10. We also give the ratio of hot spot volume emissivity to jet emissivity (assuming uniformly filled emission from both the jets and the hot spots). The volume emissivity either stays approximately constant or drops in the hot spots, compared to the jet; the increase in surface brightness is due to the longer path length. We also show the sidedness ratios of the hot spots; the hot spots are remarkably symmetric, with a mean surface brightness ratio of 1.5. Finally, we give the minimum pressures for the hot spots; all of the hot spots are resolved. These numbers indicate that the hot spots have pressures comparable to the surrounding ICM.

The hot spots in the survey not associated with bends of the tails are those in 0043+201 (which may be projected), 0110+152 (where the jets seem to continue into the lobes), and 0908−103 which exhibits rather continuous bends and a series

TABLE 3

JETS AND HOT SPOTS

Source	Brightness Ratio $\left(\frac{\text{Mean } S_{\rm jet}}{\text{Peak } S_{\rm hs}}\right)$[a]	Volume Emission Ratio $\left(\frac{\text{jet}}{\text{hotspot}}\right)$	$\left(\frac{r_{\rm hs}}{r_{\rm jet}}\right)$	Hot Spot to Core Distance (kpc)	Hot Spot Sidedness Ratio[b]	Hot Spot $p_{\rm min}$ (dyne cm^{-2})
0043+201N	0.16	2.8	9.2	65.3	1.4	3.0×10^{-12}
0043+201 S	0.18	2.0	13	64.4	...	4.3×10^{-12}
0110+152 N	0.14	44	4.0	23.3	...	1.0×10^{-11}
0836+290 S	0.44	7.0	3.2	119	...	1.4×10^{-12}
1159+583 N	0.24	0.8	1.1	17.9	1.7	4.0×10^{-11}
1159+583 S	0.72	0.2	7.5	15.0	...	2.1×10^{-11}
1231+674 N	0.32	3.1	4.2	32.8	1.3	8.6×10^{-12}
1231+674 S	0.25	10	4.0	58.9	...	5.9×10^{-12}
1306+107 N	0.04	0.2	1.7	46.2	1.8	9.0×10^{-12}
1306+107 S	0.08	0.4	0.6	34.7	...	2.1×10^{-11}
1433+553 N	0.08	0.9	6.0	31.2	1.8	1.1×10^{-11}
1433+553 S	0.13	2.4	5.3	41.2	...	7.6×10^{-12}
1636+379 N	0.66	30	11	83.5	1.2	5.7×10^{-12}
1636+379 S	0.11	1.5	2.6	81.7	...	6.1×10^{-12}
2236+176 W	1.38	4.1	3.2	38.9	1.1	1.6×10^{-11}
2236+176 E	0.56	11.13	4.8	39.0	...	1.3×10^{-11}

[a] Only sources with jets for which a mean flux density could be estimated with some confidence are included in this listing.

[b] The ratio of the surface brightness of the brighter hot spot to the dimmer hot spot. Listed for each source for which the surface brightness of each hot spot could be estimated with some confidence.

of knots in each tail instead of distinct hot spots. Of these, the hot spots that are potentially most interesting are those of 0110+152 which do not appear to be typical jet disruption points.

2.2.3. *Tails: Filaments and Substructure*

Analysis and modeling of wide angle tails has, until now, assumed uniformly filled, turbulent tails. The images in O^2E, however, show detailed, coherent structures in the tails indicating that the tails are not uniformly filled. Following Hines, Owen & Eilek (1989), we call these structures "filaments," since they tend to have a linear appearance; we do not have enough information to state definitely that they are linear structures.

The sources exhibiting reasonably well defined, measurable filamentary structures are 0110+152, 1159+583, and 1306+379. Other sources with images of similar quality do not show such organized filametary structure. Thus all WATs may not have filaments of this type. On the other hand, only three sources, 0836+290, 0908−103, and 1826+747 show no structural details in the tails. This may result from sensitivity and dynamic range limits (the images of these sources are the worst in the survey).

For the three sources with strong, resolved filaments (0110+152, 1159+583, and 1306+107) we used slices perpendicular to the filaments to measure flux densities and widths of the filaments. From these data we found minimum pressures and the volume emissivity, averaged over the filaments. We also found the emissivity and minimum pressure for the interfilament, "background," region, assuming the background is uniformly filled (the only assumption justified from the present data). The ratio of filament to background minimum pressure ranges from 2 to 7, and the ratio of filament to background emissivities ranges from 3 to 30, over these three sources. These values are similar to those found for the filaments in Cyg A (Carilli 1989) and in M87 (Hines et al. 1989).

Although the filamentary structures stand out dramatically, the interfilament regions also exhibit radio emission. This may indicate general tail emission or may arise from unresolved filaments. There are two possibilities for the distribution of the emission from the tails; it can originate from the surface of the tail, or from the entire volume which the surface encloses. The latter would be expected from the filled turbulent plumes that WAT tails have been assumed to be up to now. To distinguish between these possibilities, slices across the (resolved) tails where no filaments were present or where they were easily identified on the slice were examined for limb brightening indicative of surface emission. In general, the slices are neither straightforward cosine functions (as would be expected for uniformly filled tails), nor uniformly flat or edge brightened. This appears to eliminate the possibility that the tails are uniformly emitting volumes.

Similar possibilities exist for the filaments. They can be confined to the surfaces of the tails or distributed throughout the tail volumes. No conclusion can be reached by analysis of the current data due to the small number of filaments within any one tail.

2.2.4. *Summary: the Class Called WATs*

To end this section, we summarize what we consider the important general properties of the WAT class. We draw on the data set used in this paper, on several other well-studied WATs (3C 465, Eilek et al. 1984; 1919+479, Burns 1981; 3C 75, Owen et al. 1985; and 1313+073, Patnaik, Malkan, & Salter, 1986), on optical and X-ray data, and on general trends inferred from the cluster data set referred to above.

From all of these data, we believe that five properties correlate very well with each other and serve to delimit the class of WATs. We do not submit these as strictly defining the class of WATs, but we find that most sources satisfy most of the properties. In fact, we suspect that a source which is selected on the basis of any two properties will be likely also to satisfy the remaining three. These properties are (1) association with a dominant galaxy in the center of a cluster of galaxies; (2) a large linear size, extending $\gtrsim 50$ kpc from the radio core; (3) a dramatic jet-to-hot spot transition, as discussed in § 2.2.2; (4) large-scale bends of both tails, if any, in the same direction (C-shaped, not S-shaped); (5) radio power within a factor $\lesssim 3$ of the F-R break. In addition, these sources are not found in clusters with strong cooling cores; the radio sources associated with the central galaxies in these clusters are smaller and fainter.

3. DYNAMICS OF THE FLOW IN THE TAILS

Our primary interest in studying WATs, at this point, remains the bending problem. This requires that we analyze the flow dynamics in these sources. Since we cannot account for the complexity and diversity of all of the known sources, we base our models on a simple picture: mass and energy transport by a steady state, directed outflow in a uniformly filled jet or tail.

In order to consider the bending, we need to know the flow velocity at the bend. In the absence of direct information on the velocity field in the tail, it has become common to use the surface brightness of the tail to constrain the flow field. The basic assumption of this analysis is that the energy radiated by the plasma is supplied from the galactic nucleus by the bulk flow. (Appendix A summarizes our view of the flow paradigm for F-R I radio galaxies).

Consider a plasma flow or beam, with cross section radius r, velocity, v, density $\rho = nm_p$, thermal gas pressure $p_{\rm th}$, relativistic particle pressure $p_{\rm rel}$, and magnetic pressure $p_B = B^2/8\pi$. It has a net energy flux,

$$L_j = \pi r^2 v(\tfrac{1}{2}\rho v^2 + \tfrac{5}{2}p_{\rm th} + 4p_{\rm rel} + 2\xi p_B) \qquad (2)$$

where the factor ξ depends on the detailed magnetic field geometry (see Appendix A). We have written this for a subrelativistic flow, consistent with our argument above that $v_0 \lesssim 0.2c$. Two limits of this have been treated in the literature.

In the adiabatic limit (e.g., Fanti et al. 1982; Owen et al. 1985), the relativistic electrons which produce the observed synchrotron radiation are advected out from the galactic nucleus and suffer no in situ reacceleration. The surface brightness just reflects the deceleration of the flow, which compresses the plasma and the frozen-in magnetic field. The flow must decelerate to maintain the surface brightness in an expanding jet or tail. The relativistic electrons radiate as the plasma moves down the tail, while the thermal gas and magnetic field do not. It follows that the fraction of the total pressure, $p_{\rm tot} = p_{\rm rel} + p_B$, which comes from the relativistic particles, must decrease as a function of z (the coordinate along the tail). Also, as the relativistic electrons move down the tail, the high-energy end of the electron distribution is depleted by radiative losses, which results in a steepening of the observed synchrotron power spectrum.

In the kinetic model (e.g., Jones & Owen 1979 or Eilek et al. 1984), all the radiated energy is assumed to be supplied by the bulk kinetic energy of the flow, which is converted in situ to relativistic electrons and magnetic field, probably by turbulence or shocks in the flow. Thus, the flow must decelerate in order to transfer the bulk kinetic energy to the radiating electrons. There are no particular constraints on the internal energy in this model, except that the radiation at z must come from locally converted kinetic energy rather than advected internal energy.

This analysis can be specified to the luminosity per unit length of the tail (an easily measurable quantity). If we consider a length Δz of the tail, energy conservation requires

$$L_j(z) = L_j(z + \Delta z) + \mathscr{L}(z)\Delta z ,$$

or, in differential form,

$$\mathscr{L}(z) = -\frac{dL_j}{dz} . \tag{4}$$

Here, $\mathscr{L}(z)$ is the net loss of advected energy, both to radiation and to heating the ambient medium. Some fraction, ϵ, of $\mathscr{L}(z)$ must go to observed radio-frequency radiation: $\mathscr{L}_{\rm rad}(Z) = \epsilon\mathscr{L}(z)$. The value of ϵ will differ between the adiabatic and kinetic models. In the adiabatic model, the efficiency is determined by the fraction of the total energy flux in relativistic electrons and by the spectrum of these electrons, which determines the fraction of the particles which radiate in the local magnetic field in the observed radio band. In the kinetic model, the efficiency is determined by the fraction of the kinetic energy flux which is turned into internal or turbulent energy, and the fraction of that which is converted to relativistic electrons and magnetic field, as well as the electron spectrum which determines the radiation in the specific radio band. The coupling of the bulk flow energy to the relativistic electrons and magnetic field, is determined by the detailed microphysics (such as turbulence or shocks; see Eilek 1979).

Useful numerical estimates of these efficiencies are hard to come by. It has been common to pick $\epsilon_{\rm kin} \sim 10^{-2}$ (based, e.g., on the calculations of Eilek 1979). However, this may be optimistically large, considering the chain of energy transfer just described. If we were to guess that each step of the chain converts, say, 10% of the incoming energy to the desired channel, one might guess $\epsilon_{\rm kin} \sim 10^{-3}$ at best. We are not aware of any published estimate of $\epsilon_{\rm ad}$; our "10% per step" method suggests $\epsilon_{\rm ad} \sim 10^{-2}$ perhaps. Alternatively, energetic considerations within the adiabatic model, given in § 3.1 below, suggest that a higher value of $\epsilon_{\rm ad}$ is needed, $\epsilon_{\rm ad} \gtrsim 0.1$. We emphasize that all of these estimates are surely uncertain, and even presumptuous; we only feel comfortable in suggesting that $\epsilon_{\rm kin} < \epsilon_{\rm ad}$. In addition, the local efficiency will surely be a function of position in the tail; the global efficiency will be a function of the age of the source (e.g., Eilek & Shore 1989). However, for lack of better information, we will follow tradition and treat ϵ as a constant.

We note that this model, in either limit, assumes the flow decelerates as it moves away from the nucleus. This deceleration is probably due to entrainment of ambient matter. In the commonly held picture, these tails are subsonic or transonic flows, and turbulent entrainment seems very likely (see Bicknell 1984; De Young 1986). In support of this, we note that comparing the minimum pressure $p_{\rm min}$ values, from O^{2}E, with the typical ICM pressure, $p_{\rm ICM} \sim 10^{-11}$ dyn cm^{-2}, shows that $p_{\rm min} < p_{\rm ICM}$ in general for these sources. This is consistent with pressure confinement of the tails, and with some of the internal pressure possibly coming from entrained thermal material. Alternatively, the sum of the relativistic particle and magnetic pressure could exceed $p_{\rm min}$ if the plasma is not close to equipartition.

In this paper, we will assume the deceleration is due to entrainment, and we will further assume the plasma feels no important external force. This means we are assuming that gravitational and buoyancy forces on the tail are small. This is reasonable as long as the flow speed exceeds the typical Kepler speed in the region, which we infer from the central velocity dispersions to be roughly several hundred km s^{-1}. By comparison, our models generally consider flow speeds well above this, at least several thousand km s^{-1}. When the net force on the flow is small, entrainment will nearly conserve the momentum flux: $\pi r^2 \rho v^2$ will be approximately constant along the tail. We will use this result to simplify the algebra in the analysis which follows.

3.1. *Adiabatic Model*

The adiabatic model describes a flow in which the radio luminosity comes solely from the relativistic electrons which are accelerated in the nuclear engine. None of the flow kinetic energy (carried mostly by the higher density thermal gas) or magnetic energy is used to energize these electrons. It is worth noting that the deceleration of the flow along the tail will add the flow kinetic energy of the relativistic particles to their internal energy. Since the flow speed is much less than the random speed for these particles, this energy boost will be small and we will ignore it. (Models in which the flow kinetic energy of other species is tapped to energize the relativistic particles fall into what we call the kinetic model, which is discussed below).

To describe the overal energetics of this model, we note that only the fraction of L_j which is carried by the relativistic particles contributes to the radiation: $L_{j,\rm rel} = 4\pi r^2 v p_{\rm rel}$. Using this in equation (4), with $\mathscr{L}_{\rm rad}(z) = -dL_{j,\rm rel}/dz$, we set the total luminosity of the tail to be

$$L_{\rm rad} = \int_0^{z_{\rm max}} \mathscr{L}_{\rm rad}(z)dz . \tag{5}$$

Then, from equations (2) and (4), we get

$$L_{\rm rad} = \epsilon_{\rm ad}[4\pi r^2 p_{\rm rel} v]_0^{z_{\rm max}} \simeq \epsilon_{\rm ad}\, 4\pi r_o^2\, p_{{\rm tot},o}\, v_o \left(\frac{p_{{\rm rel},o}}{p_{{\rm tot},o}}\right) \tag{6}$$

where the subscript "o" refers to the start of the jet. In deriving this last expression, we have assumed $pv \to 0$ as $z \to z_{\rm max}$, which will be the case if the jet is decelerated or if its internal energy is used up as radiation. We have also expressed the final answer, in equation (6), in terms of $p_{{\rm tot},o}$, the total pressure at the start of the jet, which can be constrained from X-ray data. Equation (6) gives us an important constraint on the efficiency. Scaling $L_{\rm rad}$ to 10^{42} ergs^{-1} (evaluated in the usually assumed broad radio band, 10^7–10^{11} Hz, assuming an overall spectral index of 0.75; O^{2}E, Table 4), r_o to 1 kpc and the total pressure, $p_{{\rm tot},o}$ to 10^{-11} dyn cm^{-2}, and using $v_o \lesssim 0.2c$, we find a strong constraint on the efficiency in the adiabatic model:

$$\epsilon_{\rm ad} \gtrsim 0.2\, \frac{L_{42}}{r_{\rm kpc}^2\, p - 11}\, \frac{p_{{\rm tot},o}}{p_{{\rm rel},o}} \tag{7}$$

Thus, a large fraction of the advected internal energy must go into the radio band. This results suggests the internal energy

must be mostly in relativistic particles, rather than magnetic field or thermal material, and that the initial jet velocity must be close to its upper limit, $0.2c$; otherwise, an efficiency greater than unity would be required. We note that this argument requires a larger ϵ_{ad} than our guess of $\epsilon_{ad} \sim 10^{-2}$ presented above; that is, energetics considerations force us to an unexpectedly high efficiency, under the adiabatic model.

3.1.1. *Velocity Field*

In order to use this model to estimate the flow speed at the bend in each tail, we follow the approach of Owen et al. (1985). For a power-law electron distribution, $N(E) = N_0 E^{-\gamma s}$, the synchrotron emissivity per Hz and per volume goes as $j_\nu \propto N_0 B^{1/2(\gamma s+1)} \nu^{-1/2(\gamma s-1)}$.

We consider a flux-frozen magnetic field, which is oriented either parallel or perpendicular to the flow. The real field will no doubt contain both components; again we consider simple limits to test the basic model. Assuming the number of relativistic particles is conserved and taking adiabatic compression into account, we find the usual expressions for the luminosity of the beam per unit length:

$$\mathscr{L}_{\nu\parallel} \propto v^{-1/3(\gamma s+2)} r^{-1/3(5\gamma s+1)}, \quad (8)$$

$$\mathscr{L}_{\nu\perp} \propto v^{-1/3(5\gamma s+7)} r^{-1/3(7\gamma s-1)}, \quad (9)$$

as in Owen et al. 1985; Appendix B gives details of the derivation.

Polarization studies in the literature up to now have been inconclusive as to the field configuration in WATs (e.g., Ferretti et al. 1985; Patnaik et al. 1984; Burns 1981; van Breugel 1980; Burns, Owen, & Rudnick, 1979); we therefore consider both field geometries. Bridle & Perley (1984), however, note that F-R I sources tend to have *jet* magnetic fields that are either everywhere perpendicular to the jet, or which are parallel to the jet on the edges and perpendicular toward the axis. This latter case is usually interpreted as a helical field, but can also be due to a tangled field (e.g., Laing 1981).

The radius and monochromatic luminosity at 20 cm of each tail were given, as functions of position, in Paper I. We used these numbers to derive the velocity field of each tail, relative to the starting value v_0, for the parallel and perpendicular field cases. We show the results for two of the objects, 1231+674 (north tail) and 1306+107 (south tail), in Figures 2 and 3; the results are typical of all the objects. (Similar figures for all the objects can be found in O'Donoghue 1989). The velocity field derived from this model shows a strong deceleration at the hot spots; this is necessary to explain the strong increase in $\mathscr{L}(z)$ at the point where the flow widens. In the perpendicular field case, the flow decelerates by a factor of 10 to 100 at and past the hot spots in the parallel field case, the flow decelerates even more, by a factor $\gtrsim 10^4$.

With these solutions for $v(z)$, we can evaluate the time needed for a piece of plasma to be carried from the galactic nucleus to the end of the tail: $t = \int_0^{z_{max}} dz/v(z)$. We assumed $v_0 = 0.2c$ in each case. These values are given in Table 4 for each source. The "end of the tail," z_{max}, was taken to be the point where the 20 cm surface brightness dropped below the noise. We find that the travel times for the parallel field case generally exceed the age of the universe; we do not consider this case further. The perpendicular field case predicts travel times $\sim 10^7$ to 10^8 yr, which does not violate any a priori constraint.

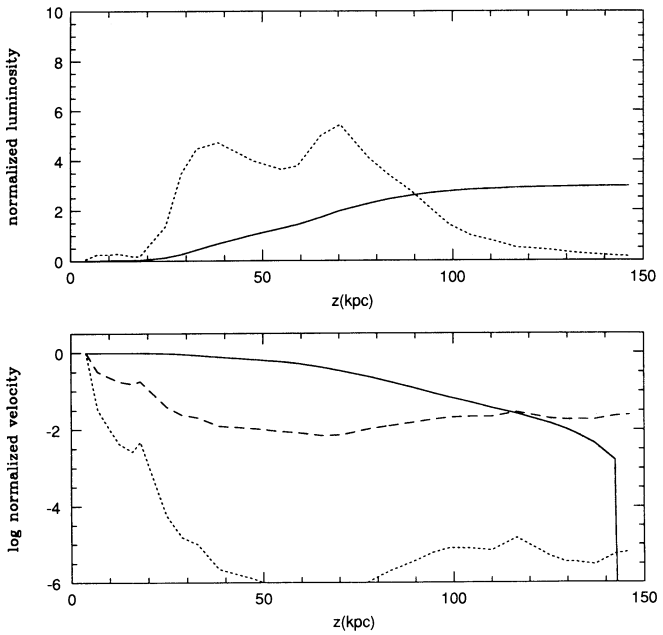

FIG. 2.—(*a*) The luminosity per slice, $\mathscr{L}(z)$ (*dotted line*), and the total luminosity out to z, $L(z) = \int_0^z \mathscr{L}(z)dz$ (*solid line*), for the north tail of 1231+674. (*b*) The velocity curves derived from $\mathscr{L}(z)$, for the adiabatic model assuming perpendicular (*dashed line*) and parallel fields (*dotted line*), and for the kinetic model (*solid line*).

3.1.2. *Spectral Aging*

We can derive an independent estimate of the travel time down the tail, in the adiabatic model, from the observed radio spectrum. As in other F-R I sources, we found that the spectrum steepens going out along the tail (O^2E gives the spectral index between 6 and 20 cm as a function of position for each source).

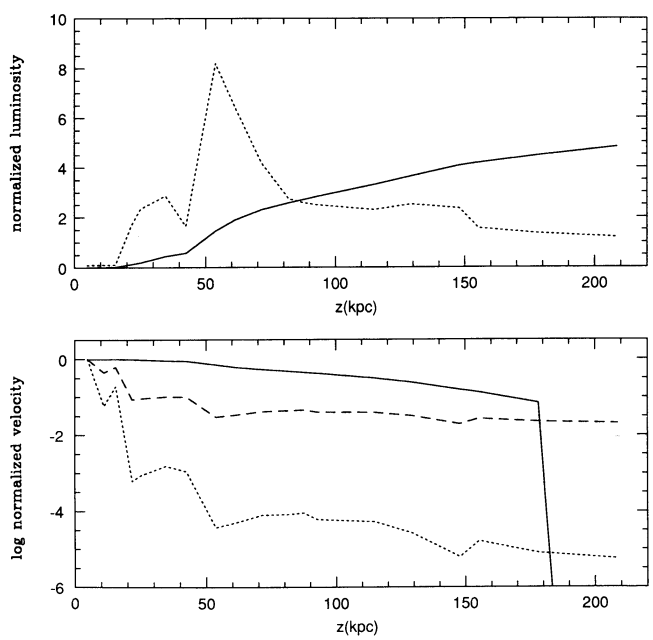

FIG. 3.—The same as Fig. 2, for the south tail of 1306+107

TABLE 4

PARTICLE TRAVEL TIMES

SOURCE	LENGTH (kpc)	TRAVEL TIME[a]				
		Adiabatic		Spectral Aging		
		B_{par}	B_{perp}	B_C	$B_{min\ p}$	Kinetic
0043+201 N	205	2.3×10^6	220	34	12	20
0043+201 S	229	2.4×10^6	260	30	13	23
0110+152 N	205	4.0×10^6	310	35	13	86
0110+152 S	184	2.6×10^8	860	40	13	33
0836+290 N	317	7.5×10^6	240	26	8	17
0836+290 S	382	3.3×10^5	170	21	11	36
0908−103 N	270	6.4×10^5	120	26	14	21
0908−103 S	277	1.5×10^6	140	18	8	20
1159+583 N	40	4.1×10^5	40	23	3	2.3
1159+583 S	107	2.6×10^2	6.3	19	3	20
1231+674 N	130	1.4×10^6	140	35	8	160
1231+674 S	126	1.5×10^6	140	23	5	21
1306+107 N	233	3.3×10^5	160	38	13	63
1306+107 S	209	2.3×10^5	110	35	10	18
1433+553 N	142	1.3×10^7	300	30	6	88
1433+553 S	63	1.8×10^6	83	23	5	5.9
1636+379 N	213	9.4×10^7	600	17	3	240
1636+379 S	233	6.0×10^3	36	29	26	210
1826+747 W	378	3.9×10^3	38	29	14	69
1826+747 E	291	5.9×10^4	90	35	15	77
2236−176 W	106	9.8×10^4	42	28	7	6.9
2236−176 E	125	8.3×10^6	230	3.8	0.6	150

[a] In millions of years.

In a source with an initial power-law electron spectrum, and no in situ reacceleration, the particle spectrum steepens, at time t, for energies given by

$$c_2 E \int_0^t B^2(\tau) d\tau \gtrsim 1 , \quad (10)$$

where the integral is taken over the lifetime of the plasma, and $c_2 = 2e^4/3m_e^2 c^7$ (Pacholczyk 1970). This produces a steepening in the photon spectrum at a frequency

$$\nu_{break} = \frac{c_1}{c_2^2} \frac{B(t)}{B_{rms}^4 t^2} \quad (11)$$

where $c_1 = 3e/4\pi m_e^3 c^5$, and we use the rms field $B_{rms}^2 = t^{-1} \int_0^t B^2(\tau) d\tau$. A more complete analysis includes the redshift of the source, z_R, and the inverse Compton losses due to the microwave background (the latter through the Compton equivalent field, $B_c = 4(1 + z_R)^2 \mu$G; van der Laan & Perola 1969). Including these factors and inverting (11), we relate the lifetime out to position z to the break frequency at the point:

$$t(z) = 3.35 \times 10^4 \frac{B(z)^{1/2}}{(B_{rms}^2 + B_c^2)} \frac{1}{[(1 + z_R)\nu_{break}]^{1/2}} \text{ yr} \quad (12)$$

where $t = \int_0^z dz/v(z)$ relates the travel time to the distance down the tail; equation (12) uses B in Gauss, and ν in Hz. (Details of this are given in Appendix C.)

For each source, we estimate ν_{break} from the parameter, $X = (\nu/\nu_{break})^{1/2}$. We used the numerical values in Figure 4, in Appendix C, to relate the spectral index observed between 6 and 20 cm to the local break frequency, $\nu_{break}(z)$. We picked two models for the magnetic field in equation (12): one assuming $B = B_c$ everywhere, and another taking the minimum-pressure field at each point (see O^{2}E). This allowed us to find the lifetime of the electrons at points z in the tail, and thus the travel time to the end of the tail. These values are also given in Table 4. We immediately see a major contradiction: the travel times based on spectral aging are at least a factor of 10 shorter than the travel times based on the adiabatic model, with the perpendicular field assumption. This contradiction was pointed out by Owen et al. (1985) for 3C 75; we find that it holds for these sources as well.

3.1.3. *Is the Spectral Aging Analysis Right?*

The results of the previous section find a severe lifetime problem with the adiabatic model: the lifetime predicted from the spectral steepening is much shorter than the travel time inferred from the velocity field. Owen, Hardee, & Cornwell (1989) suggested one way to alleviate a similar lifetime problem in the jet of M87. They suggested that most of the volume of the jet is filled with a very low magnetic field, $B \gg B_c$, so that the electron radiative losses are minimized during their travel down the jet. Most of the synchrotron luminosity is argued to arise from a high field region, for instance on the surface of the jet. Owen et al. note that such a boundary layer could arise in M87 from various surface interactions, and may be observed in the filamentary synchrotron emissivity; similar arguments might be made for the tails we are considering here. If this is the case, then at some point z down the tail, some of the electrons may scatter into the high-field region, and radiate there at a higher frequency than they would in the "hollow" core of the tail. This increases the value of the break frequency that would be observed, for a given lifetime t.

From our discussion in Appendix C, we note that this effect can be incorporated simply in equation (12). The rms field seen by the particle over most of its travel time is assumed to be small: $B_{rms} \ll B_c$. The "local" field that the particle scatters into, $B(z) = B_{high}$, is then high compared to B_c and B_{rms}. The age of the electrons seen at z is then raised, over the homoge-

neous aging model of § 3.1.2, by

$$\frac{t_{\rm hollow}}{t_{\rm uniform}} = \left(\frac{B_{\rm high}}{B_{\rm rms}}\right)^2 \frac{B_{\rm rms}^2 + B_c^2}{B_c^2} \tag{13}$$

Clearly, this model helps the lifetime problem if $B_{\rm high} \gg B_{\rm rms}$. In § 3.1.2 we took $B_{\rm rms} = B_c$, or found the rms value of the minimum-pressure field; the latter came out to be a few times B_c. Unlike the M87 jet, there is no evidence in these WATs that the tails are overpressured with respect to their surroundings. Thus, the highest likely value for $B_{\rm high}$ is probably that required for pressure equilibrium with the surrounding ICM: $B_{\rm PE} = (8\pi p_{\rm ICM})^{1/2} \simeq 16$ μG if $p_{\rm ICM} = 10^{-11}$ dyn cm^{-2}. This value is not that much greater than $B_{\rm rms}$. We therefore find the estimated lifetimes, in this "hollow tail" picture, will be a few times greater than those estimated above, which is not enough to help the inconsistencies in the adiabatic model as we have considered it.

3.2. *Kinetic Model*

The kinetic model assumes that some fraction, $\epsilon_{\rm kin}$, of the kinetic energy flux is converted in situ to observed radiation, and ignores any advected energy:

$$\mathscr{L}_{\rm rad}(z) = -\epsilon_{\rm kin} \frac{d}{dz}\left(\frac{1}{2}\pi r^2 \rho v^3\right). \tag{14}$$

Note that the efficiency in this equation may have a very different numerical value from that in equation (6) (as discussed after eq. [4]). We suspect $\epsilon_{\rm kin} \ll 1$ in the kinetic model.

We describe the overall energetics of this model by integrating equation (4) along the tail, this time keeping only the kinetic term. This recovers the usual global energy condition,

$$L_{\rm rad} = \epsilon_{\rm kin}(\tfrac{1}{2}\pi r^2 \rho v^3)_0^{z_{\rm max}} \simeq \tfrac{1}{2}\epsilon_{\rm kin}\pi r_o^2 \rho_o v_o^3 \tag{15}$$

If we assume $v \to 0$ as $z \to z_{\rm max}$. Using the same scaling as in equation (7), and again taking $v_o \lesssim 0.2c$, we find the condition,

$$\epsilon_{\rm kin} n_o \gtrsim 2 \times 10^{-7} \frac{L_{42}}{r_{\rm kpc}^2} \tag{16}$$

Taking $\epsilon_{\rm kin} \sim 10^{-3}$ as a "reasonable guess," this does not put any strong constraint on the jet density: $n_0 \gtrsim 0.1 n_{\rm ICM}$ is needed if $L_{42}/r_{\rm kpc}^2 \sim 1$.

3.2.1. *Velocity Field*

To derive $v(z)$ from the data, we use equation (4) in this limit and assume the momentum flux, $\rho v^2 r^2$, is constant. We get

$$\mathscr{L}_{\rm rad}(z) = \frac{1}{2}\epsilon_{\rm kin}\pi r_o^2 \rho_o v_o^2 \frac{dv}{dz}, \tag{17}$$

where we have evaluated the constant at the base of the flow. We can combine this with (15) and rearrange terms to get

$$\frac{dv}{dz} = -\frac{v_o}{L_{\rm rad}} \mathscr{L}_{\rm rad}(z). \tag{18}$$

This then integrates to

$$v(z) = v_o\left[1 - \frac{1}{L_{\rm rad}}\int_0^z \mathscr{L}(z)dz\right]. \tag{19}$$

Again, we have fixed the integration constant in equation (19) by assuming $v \to 0$ as $z \to z_{\rm max}$.

We used equation (19) to derive $v(z)/v_o$ for each source in this model. Figures 2 and 3 show this result for 1231+674, north tail, and 1306+107, south tail, which are again typical of all the sources. The velocity field predicted by this model decays slowly from the start to the end of the flow. [The sharp drop in $v(z)$ at the end of the tail is artificial, due to our forcing v to zero at the end of the luminous tail.] In the kinetic model we have no a priori constraint on the density, ρ_o, in equation (15). Therefore, the starting velocity, v_o, is less tightly constrained by the energetics in this model than in the adiabatic model (see eq. [6]), where we have observational constraints on the total pressure, $p_{{\rm tot},o}$. Nonetheless, thinking of the sidedness arguments in § 2.2.1, we pick $v_o = 0.2c$ here, which allows us to compare this model with the adiabatic model. Using this value, we evaluated the travel times to the end of the tail for each source, and they are given in Table 4. Since the velocity of this model does not decelerate as dramatically early in the flow as it does in the adiabatic model, the mean velocity in the tail is higher, and the travel times shorter, than in the adiabatic model.

We see no obvious problems with this velocity field, and we have not found any other "consistency" tests for the kinetic model (akin to the spectral aging test for the adiabatic model). We also retain hope that the aging problem in the adiabatic model may be circumvented (see § 5 below). Therefore, we use both of these models to test the bending condition for these sources.

4. BENDING WIDE-ANGLE TAILED RADIO SOURCES

Having explored the dynamics of the tails, and derived velocity fields from the adiabatic and the kinetic models, we can now use these to evaluate the bending. That is, we consider whether the ram pressure acting on jet due to the slow motion of the galaxy relative to the ICM can bend jets described by either of these two models.

4.1. *Ram Pressure Bending*

Although various bending mechanisms were considered in Eilek et al. (1984), ram pressure bending seems the most likely to be consistent with the subsonic, fluid picture of these sources. Of the other possibilities discussed in that paper, we note that electromagnetic forces would require a beam with a strong net current, and a strong magnetic field in the ICM localized at the bend: this may be possible but involves a quite different picture than is currently accepted for these sources. The possibility of collisions of the beam with dense clouds seems unlikely; De Young (1990) simulates this and does not reproduce WAT structure. In addition, Owen, O'Dea, & Keel (1990) searched for such clouds in 3C 465 and 3C 75 and put restrictive upper limits on any such clouds. We therefore restrict ourselves to consideration of ram pressure bending: can the pressure gradient exerted by the relative motion of the galaxy and the ambient medium account for the geometry of these sources?

The bending of a fluid beam must be described by Euler's equation (see Appendix A). The pressure gradient due to ram pressure bending is usually approximated as $\nabla p \simeq \rho_{\rm ICM} v_g^2 / l_{\rm pressure}$, if v_g is the relative velocity between the ICM and the galaxy, and $l_{\rm pressure}$ is the scale height of this pressure gradient. In calculations, we will assume $l_{\rm pressure} \simeq r_b$, the beam radius at the bending point; this assumes an unshielded beam and gives the strongest bending. Euler's equation in this

approximation is

$$\rho \frac{v^2}{l_{\rm bend}} \simeq \rho_{\rm ICM} \frac{v_g^2}{l_{\rm pressure}} \quad (20)$$

if $l_{\rm bend}$ is the scale over which the beam bends.

As De Young (1990) has emphasized, this equation can be used to describe the bending only if ρ and v are evaluated as averages throughout the region where the force is exerted and the flow actually bends. In particular, the flow may decelerate due to entrainment of mass; the velocity at the bend may be much less than that at the start of the jet, v_o. We will use the velocity fields deduced for the adiabatic and kinetic models in § 3, to estimate the velocity at the bend; we call $\rho(z_{\rm bend}) = \rho_b$ and $v(z_{\rm bend}) = v_b$. In addition, equation (20) is valid only if the flow velocity is approximately constant throughout the region where the flow actually bends. In most of our sources, the bend seems to happen over a short distance, $\Delta z \ll z_{\rm bend}$, so this is probably not too bad an approximation. In sources where $\Delta z \sim z_{\rm bend}$, however, some mean of ρv^2 throughout the bend must be used in equation (20).

Knowing the velocity field at the bend is not enough to test this ram pressure bending model; equation (20) still has three unspecified quantities, ρ_b, v_o, and v_g. We estimate these quantities as follows: In the adiabatic model, we use equation (6) to find v_o in terms of $p_{{\rm tot},o}$ (which we estimate from the X-ray data, as above), $L_{\rm rad}$ and $\epsilon_{\rm ad}$ (which we expect to be fairly large, as in § 3.1 above). We pick v_g to be 100 km s^{-1}, which is typical of observational limits on the velocities of central dominant cluster galaxies relative to the center of mass of the cluster, as discussed above. We then use equation (20) to ask what density of beam can be bent by ram pressure. Equation (20) evaluates ρ_b, the density at the bend; we use the measured r_b/r_o ratio, and the estimated v_b/v_o ratio, to determine the initial beam density that is consistent with ram pressure bending, ρ_o (assuming entrainment with conservation of momentum flux). The analysis is a bit simpler for the kinetic model. We use (15) to express ρ_o in terms of v_o, $L_{\rm rad}$ and $\epsilon_{\rm kin}$ for kinetic beams. We take $v_o = 0.2c$, which makes the beams easiest to bend, since the inertia term in (20) $\propto L_{\rm rad}/v_o$ in this model. We relate conditions at the bend to the initial conditions by noting that the mass flux in the beam cannot decrease, if the beam is entraining matter. This gives us a lower limit for the product of $v_g \epsilon_{\rm kin}^{1/2}$ that can satisfy the ram pressure bending condition in these beams.

4.2. *Bending in the Adiabatic Model*

We incorporate the velocity field analysis by rewriting equation (20) as

$$\frac{\rho_b}{\rho_{\rm ICM}} = R_b \left(\frac{v_g}{v_o}\right)^2 \quad (21)$$

where

$$R_b = \left(\frac{l_{\rm bend}}{l_{\rm pressure}}\right)\left(\frac{v_o}{v_b}\right)^2$$

is evaluated at the bend. For each tail with significant bends (17 of the 22), we determined the location of each bend, $z_{\rm bend}$, the beam radius there, $r_b \simeq l_{\rm pressure}$, and used the $v(z)$ derived from the perpendicular magnetic field assumption, to evaluate R_b.

In order to ask whether the sources can satisfy equation (21), we must constrain some of the unknowns. To this end, we pick $v_g = 100$ km s^{-1}, from observed limits on galaxy velocities in clusters, and we use equation (6) to write v_o in terms of p_o, $L_{\rm rad}$ and $\epsilon_{\rm ad}$ as above. With the same scaling as in equation (7), and picking $\gamma_A = 4/3$ (since we will derive low beam densities, suggesting they may be internally relativistic), we find

$$\frac{\rho_b}{\rho_{\rm ICM}} \simeq \zeta_{\rm ad}(\epsilon_{\rm ad} p_{-11})^2 \quad (22)$$

where $\zeta_{\rm ad} = 1.3 \times 10^{-4}(R_b/L_{42}^2)$. This is the condition under which beams can be bent by ram pressure in the adiabatic model. For each source, we evaluate $\zeta_{\rm ad}$, using half of the single-dish flux for L_{42} (see Table 1). The relevant bending scales and dimensionless quantities are collected in Table 5 for each source with a significant bend. We argued above, from energetics, that $\epsilon_{\rm ad}$ cannot be too small; $10^{-2} \lesssim (\epsilon_{\rm ad} p_{-11})^2 \lesssim 1$ might be a possible range. From the values of $\zeta_{\rm ad}$ in Table 5, we see that beams with ρ_b much less than $\rho_{\rm ICM}$, say by a factor $\sim 10^3$ to 10^5, are necessary to account for the bending.

Are such low densities at the bend reasonable? We check this by assuming the deceleration of the flow results from

TABLE 5

BENDING TAILS IN THE ADIABATIC MODEL

Source	z_b (kpc)	r_b (kpc)	l_b (kpc)	v_b/v_o	$\zeta_{\rm ad}$	ρ_b/ρ_o	$\zeta_{\rm ad}\rho_o/\rho_b$
0011+152 N	119	8.2	44	0.0076	1.8	260	0.69
0836+290 N	75.3	2.2	12	0.22	0.0096	4.3	0.0023
0836+290 S	103	6.0	33	0.28	0.0061	0.36	0.017
1159+583 N	14.1	1.6	9.8	0.035	0.28	3.2×10^4	8.8×10^{-6}
1159+583 S	25.3	1.0	16	2.1	2.0×10^{-4}	0.22	8.8×10^{-4}
1231+674 N	18.0	1.2	16	0.18	0.024	23	0.0011
1231+674 S	21.5	1.6	25	0.11	0.084	37	0.0030
1306+107 N jet	20.6	0.53	22	9.6	7.7×10^{-6}	0.038	2.0×10^{-4}
1306+107 N tail	78.1	7.1	21	0.16			
1306+107 S	148	11	45	0.019	0.019	21	8.9×10^{-4}
1433+553 N	55.4	5.2	4.6	0.064	0.14	9.1	0.015
1433+553 S	29.5	1.8	9.5	0.020	0.82	790	0.0010
1636+379 N	43.0	2.3	170	0.097	0.19	20	0.0093
1636+379 S	15.6	4.0	43	0.98	2.9×10^{-4}	0.065	0.0043
1826+747 W	29.3	2.3	28	1.1	7.1×10^{-4}	0.15	0.0047
1826+747 E	37.6	2.6	56	0.22	0.035	3.2	0.011
2236−176 E jet	14.4	0.74	47	0.17	0.21	65	0.0032
2236−176 E tail	42.5	4.3	16	0.013	2.0	300	0.0066

entrainment which conserves the momentum flux, so that $\rho_b v_b^2 r_b^2 = \rho_o v_o^2 r_o^2$. The measured r_b/r_o ratios (scaled to $r_o = 1$ kpc), and the v_b/v_o values deduced from the model, then give the density changes, ρ_b/ρ_o; these values are also listed in Table 5. [Some of the ρ_b/ρ_o values are inferred to be less than unity; these come from sources which spread rapidly without a strong increase in the strip brightness, $\mathscr{L}(z)$]. Thus, these beams bend if the ratio of the initial beam density to the ambient density is given by

$$\frac{\rho_o}{\rho_{\rm ICM}} = \zeta_{\rm ad} \frac{\rho_o}{\rho_b} (\epsilon_{\rm ad} p_{-11})^2 .$$

Still assuming $\epsilon_{\rm ad}$ is not too small, we conclude that beams which start with $\rho_o/\rho_{\rm ICM} \lesssim 10^{-3}$ are necessary to account for the bent tails in WATs, under this model. While these values are low, we do not see that they conflict with anything. Thus, the strong deceleration predicted by the adiabatic model will allow low-density beams to bend and produce sources which resemble WATs. The problem with this model, as above, is the apparent inconsistency of the inferred velocity field with the inferred spectral ages of the particles.

4.3. *Bending in the Kinetic Model*

We begin this analysis with the basic bending equation (20), evaluated at the bend. The kinetic model predicts less deceleration by the bending point, so that v_b/v_o is larger there than in the adiabatic model. We expect this will make the beams harder to bend under the kinetic model.

We apply equation (20) by including the global energy balance, equation (15). With this, it is simple to show that beams which supply $L_{\rm rad}$ in kinetic energy cannot be bent by ram pressure, as follows. In order to relate conditions at the bend to conditions at the origin of the jet, we use the condition that the mass flux down the beam will increase if the flow decelerates by entrainment: $\rho_b v_b r_b^2 > \rho_o v_o r_o^2$. With this, we write equation (20) as

$$\rho_{\rm ICM} v_g^2 > \rho_o v_o^2 \left(\frac{r_o^2}{r_b l_{\rm bend}} \right) \frac{v_b}{v_o}$$

We now incorporate the total luminosity condition, equation (15). This eliminates $\rho_o r_o^2$ and leaves only one "unknown" on the right-hand side, v_o. Putting in the numerical scaling, we have

$$\rho_{\rm ICM} v_g^2 > \frac{0.22}{\epsilon_{\rm kin} v_o} \zeta_{\rm kin} \qquad (23)$$

where $\zeta_{\rm kin} = (L_{42} v_b / l_{\rm bend,kpc} v_o)$, and $\rho_{\rm ICM}$, v_o and v_b are in cgs units. The lowest v_g needed to bend the beam clearly comes from the largest allowed v_o, which we argued is $\simeq 0.2c$. Using this and $\rho_{\rm ICM} = 10^{-3} m_p$ gives the lowest v_g which can bend the flow in this model. These lower limits are given in Table 6, along with the scales and $\zeta_{\rm kin}$ values for each source. Since we expect $\epsilon_{\rm kin} \lesssim 10^{-2}$, we see that v_g must exceed several thousand km s^{-1} in order to bend the tails in this model. Thus, this larger data set confirms that models in which the radio luminosity of WATs is supplied, at low efficiency, from the bulk flow kinetic energy cannot be bent as observed by the motion of the parent galaxy through the intracluster medium.

TABLE 6

BENDING TAILS IN THE KINETIC MODEL

Source	z_b (kpc)	r_b (kpc)	l_b (kpc)	v_b/v_o	$\zeta_{\rm kin}$	min $(v_g \epsilon_{\rm kin}^{1/2})$ (km s^{-1})
0110+152 N	119	8.2	44	0.18	0.011	150
0836+290 N	75.3	2.2	12	0.85	0.087	430
0836+290 S	103	6.0	33	0.84	0.031	260
1159+583 N	14.1	1.6	9.8	0.93	0.14	560
1159+583 S	25.3	1.0	16	0.55	0.054	340
1231+674 N	18.0	1.2	16	0.99	0.094	450
1231+674 S	21.5	1.6	25	0.98	0.059	360
1306+107 N jet.....	20.6	0.53	22	1.0	0.13	520
1306+107 N tail.....	78.1	7.1	21	0.43	0.0054	340
1306+107 S	148	11	45	0.16	0.0094	140
1433+553 N	55.4	5.2	4.6	0.54	0.017	190
1433+553 S	29.5	1.8	9.5	0.91	0.14	550
1636+379 N	43.0	2.3	170	0.99	0.014	170
1636+379 S	15.6	4.0	43	0.99	0.053	340
1826+747 W	29.3	2.3	28	0.89	0.041	300
1826+747 E	37.6	2.6	56	0.78	0.018	200
2236−176 E jet	14.4	0.74	47	0.98	0.025	230
2236−176 E tail	42.5	4.3	16	0.82	0.061	360

5. CONCLUSIONS AND DISCUSSION

We have presented two major results in this paper.

The first is that we believe WATs form a distinctive subset of F-R type I sources. A WAT is a large, high-power, C-shaped F-R type I source, attached to a dominant cluster-center galaxy, which has a dramatic jet-to-hot spot transition. These five properties seem to be well correlated with each other, and set the WATs apart from other F-R type I sources.

Our second conclusion is that current models of the physics of these sources do not work. The pure kinetic model cannot account for the bending of the beams. The inertia in the flow, required if the kinetic energy flux is to account for the radio luminosity, cannot be bent by the ram pressure due to the slow galaxy motion relative to the cluster. Nor does the pure adiabatic model work. We find that low-density ($n_o \lesssim 10^{-3} n_{\rm ICM}$) beams, which supply the radio luminosity by advected internal energy, can be bent by ram pressure in these sources. However, the strong deceleration needed to explain the surface brightness in these models requires travel times much longer than the single particle lifetimes.

Our conclusion that the kinetic model cannot account for the bending of these sources has an important consequence. We find that radio tails whose power is provided by kinetic energy flux cannot be bent by ram pressure in these environments. However, these sources are often bent. Therefore, their radio power cannot be entirely provided by their kinetic energy flux. This contradicts a common assumption in the field, namely, that the Mach number (which is considered to measure the kinetic energy flux) determines the radio power. We have only established this for WATs, where the bending provides a test of the assumption that power correlates with Mach number. This makes us wonder, however, whether the higher power of F-R type IIs is due mainly to their being supersonic, as is commonly assumed.

What is the next step? We first note limitations of both of these "standard" theories which have become clear to us, then we present some possible alternative models which may merit further exploration.

One clear problem with the standard, steady-flow model presented in this paper is the necessity to work in only the

adiabatic, or only the kinetic, limit. Equations (2) and (4) clearly show that both advected internal energy, and internal energy "created" locally (by in situ conversion of kinetic energy flux) should be important; it is not simply the local Mach number, but also the local deceleration, that determines which of the two terms is important. It is very likely that both of the terms will be important, somewhere along a given tail.

In addition, the analysis of Eilek & Shore (1989) shows that the locally "created" internal energy will be radiated at a rate determined by the local magnetic field and electron energy. If the local flow rate is greater than this radiation rate, the "created" internal energy will not be radiated locally, but will add to the advected internal energy budget.

We also note that these models do not address the dynamics of the flow. Although Bicknell (1984; see also Bicknell et al. 1990) rather successfully predicted the surface brightness evolution of jets from the spreading rate by modelling the turbulent flow, his work did not address the dramatic broadening, brightening and bending seen in WATs. He makes the point that detailed modelling requires knowledge of the turbulent stresses in the flow, as well as the pressure profile of the galactic atmosphere. Thus the deceleration of a turbulent radio jet cannot easily be predicted from basic dynamical principles.

In addition, the sources are unlikely to be well represented by steady state models, with constant efficiencies. They must be evolving both in size and in brightness (see Eilek & Shore 1989). The efficiency—which has become a standard fudge factor in these analyses—is very likely to be both a function of time (as the source evolves) and a function of position (due to the changing internal state of the plasma). Since we do not know how to address this question in this context, we have assumed constant efficiencies, but we find this unsatisfying.

It may be that the standard model (as presented thus far in the paper, and which we summarize as the "flow paradigm" in Appendix A), if extended in the ways just described, will account for the sources. However, there are several alternative models which we find attractive.

Can the lifetime problems in the standard model be overcome? We found, above, that the "hollow tail," in which the relativistic electrons move at the flow speed, but in regions of very low magnetic field, cannot extend the particle lifetimes by enough in these sources to overcome the problem. Is it possible that the electrons stream through the slowly moving bulk plasma? If they can move much faster than the bulk speed inferred from the surface brightness in the adiabatic model, the lifetime problem might be alleviated. In order to do this, they must not be slowed down by the streaming instabilities which limit the relative speed of an electron beam to roughly, the Alfvén speed of the plasma (e.g., Wentzel 1974). In order to avoid streaming instabilities, this picture implies the sources are highly inhomogeneous, with both the density and magnetic field varying throughout the source.

Alternatively, the energy might be supplied through some means other than kinetic energy flux down the jet. This would allow some in situ energization at the hot spots, and possible coupling to a mainly adiabatic model further out. One way to do this is for the surrounding gas (the ICM) to provide an energy source—the local ICM has some level of turbulence (e.g., Hu, Cowie, & Wang 1985; or Owen, Eilek, & Keel 1993; on the evidence for transonic random motions in the hot ICM). This turbulence, which may include a field of randomly propagating sound and Alfvén waves, may "stir up" the plasma in the radio tails. this "stirring" could, perhaps, excite Alfvén waves in the tails, which could accelerate the electrons in situ.

Another alternative idea is that the energy comes from a current system in the radio sources. this is not a new idea (e.g., Bedford 1978; Eilek 1984; Borovsky 1986). The ordered, luminous filaments seen in some of our sources may well be local regions of field-aligned current. This would provide an energy source internal to the radio galaxy, and presumably driven by the dynamos in the core, but which is not coupled to the kinetic energy flow. This hypothesis is, unfortunately, hard to test quantitatively, since the magnitude of the energy transport is sensitive to microscopic transport coefficients (such as the electrical conductivity), which are probably anomalous (see the discussion in Hines et al. 1989; also Borovsky 1986).

We present the above alternative ideas only as hypotheses. None have been investigated quantitatively, or really even physically in any detail. Our main point is, we feel a new approach may be needed to the physics of these sources.

We thank Jack Burns, Dave De Young and Jun-Hui Zhao for helpful discussions. Our referee, Geoff Bicknell, contributed important comments which have strengthened the paper. The work of J. E. was supported in part by NASA grant NAGW-1591.

APPENDIX A

THE FLOW PARADIGM

A.1. USE OF HYDRODYNAMIC MODEL

The picture of the beams that has emerged from the model first put forth by Blandford & Rees (1974), is the outflow of an electrically neutral collisionless plasma from the galactic core that transports mass, energy, and momentum to the extended radio components. The energy carried by the beam is required to supply the radiated energy detected as emission from the jets and from the more extended lobes and tails. Although the plasmas are tenuous, with Coulomb mean free paths much greater than the source scale sizes, the embedded, probably tangled, magnetic fields result in Larmor radii much smaller than the scale size. In addition, microturbulent scattering of particles from plasma waves may both act in reducing the collision length so that a fluid model is appropriate (e.g., Bicknell & Melrose 1982; Eilek & Shore 1989). The plasma is generally thought of as thermal and internally subrelativistic; it must also contain the relativistic electrons, which radiate, and possibly also relativistic ions which were accelerated in the same process as accelerated the electrons. These relativistic particles are assumed to be tied to the thermal plasma by the same microturbulence and small-scale tangled magnetic fields, so that they propagate at the same flow speed.

Within this picture, the energy and momentum transport in the beam can be expressed in terms of the usual fluid variables. We follow Landau & Lifshitz (1959) and Bateman (1976) for the general equations, and O'Dea (1984) for the application to radio sources. We assume the bulk flow speed of the beam is subrelativistic.

A.2. THE ENERGY FLUX

The energy density of the plasma in the beam can be written,

$$u_{\rm tot} = \frac{1}{2}\rho v^2 + u_{\rm int} + \frac{B^2}{8\pi}, \tag{A1}$$

where ρ is the mass density of the beam, v is the bulk velocity, B is the magnetic field, and the internal energy density is $u_{\rm int} = u_{\rm rel} + u_{\rm th}$, the sum of the internal energies in relativistic particles ($u_{\rm rel}$) and in thermal material ($u_{\rm th} = (3/2)nk_B T$). Considering the material in the beam as an ideal fluid, we write the time rate of change of the energy density at a fixed point in space as

$$\frac{du_{\rm tot}}{dt} = \frac{\partial}{\partial t}\left(\rho\frac{1}{2}v^2 + u_{\rm int} + \frac{B^2}{8\pi}\right) + \nabla\cdot\left[\rho\boldsymbol{v}\left(\frac{1}{2}v^2 + w\right) + \frac{\boldsymbol{E}\times\boldsymbol{B}}{4\pi}\right] = -l, \tag{A2}$$

where l is the net energy loss rate per volume, sinks minus sources, from the plasma (say, due to radiative losses and entrained internal energy), and $\boldsymbol{E}\times\boldsymbol{B}/4\pi$ is the Poynting flux. In equation (A2), w is the enthalpy which, in the explicit form

$$\rho w = u_{\rm int} + p_{\rm int} \tag{A3}$$

can be seen to include in the energy flux not only the internal energy the fluid carries with it, but also the work done on the fluid by the surrounding pressure. The internal energy and pressure are related, for each species (relativistic and nonrelativistic), as $u_{\rm int} = p_{\rm int}/(\gamma_A - 1)$, where γ_A is the adiabatic index. For a thermal particle dominated plasma, $\gamma_A = 5/3$, while $\gamma_A = 4/3$ for a plasma which is internally relativistic. The quantity operated upon by the divergence in (A2) is the energy flux vector and describes the rate of energy crossing a unit area of surface perpendicular to the velocity. Specializing to flow along the jet (in the $\hat{z}$-direction), ignoring variation of all parameters across the jet, and letting the component of magnetic energy flux along the jet be $\xi v B^2 = [B^2\boldsymbol{v} - (\boldsymbol{v}\cdot\boldsymbol{B})\boldsymbol{B}]_z$, we write the net rate of energy flowing along the jet as

$$L_j = \pi r^2 v\left(\frac{1}{2}\rho v^2 + u_{\rm int} + p_{\rm int} + \xi\frac{B^2}{4\pi}\right). \tag{A4}$$

Jets in which the first term in the parentheses dominates would be described by the kinetic model; those in which the internal energy dominates would be described by the adiabatic model. Since the ratio of the kinetic energy density to the internal energy density is proportional to the Mach number squared in simple fluids (where the Mach number is defined as the ratio of the flow speed to the sound speed), jets described by the kinetic model can be thought of as high Mach number flows, while adiabatic jets can be thought of as low Mach number flows (e.g., O'Dea 1984).

A.3. MOMENTUM FLUX

The rate of change of momentum of a unit volume of fluid is

$$\frac{d}{dt}(\rho\boldsymbol{v}) = \frac{\partial}{\partial t}(\rho\boldsymbol{v}) + \nabla\cdot(\rho\boldsymbol{v}\boldsymbol{v}) = -\nabla p_{\rm ext} + \boldsymbol{F}_{\rm ext} \tag{A5}$$

where $p_{\rm ext}$ is the externally applied pressure and $\boldsymbol{F}_{\rm ext}$ is the net externally applied force. (For instance, $F_{\rm ext}$ would include gravity, bouyancy, and radiation pressure.)

The term inside the divergence in equation (A5) is the momentum flux tensor; in a steady state flow we have

$$\nabla\cdot(\rho\boldsymbol{v}\boldsymbol{v}) = \nabla p_{\rm ext} + \boldsymbol{F}_{\rm ext} \tag{A6}$$

If $\boldsymbol{F}_{\rm ext} - \nabla p_{\rm ext} \simeq 0$, the net momentum flux $\rho v^2 r^2$ is conserved along the beam.

This equation can be combined with the continuity equation,

$$\frac{d\rho}{dt} = \frac{\partial\rho}{\partial t} + \nabla\cdot(\rho\boldsymbol{v}) = s \tag{A7}$$

if s describes the net rate of gain of mass per unit volume (e.g., Mathews & Baker 1971). Combining equation (A7) with equation (A5), and again assuming a steady state, we have

$$\rho(\boldsymbol{v}\cdot\nabla)\boldsymbol{v} = -\nabla p_{\rm ext} + \boldsymbol{F}_{\rm ext} - s\boldsymbol{v}, \tag{A8}$$

which is the time-independent Euler's equation, explicitly including the effects of entrainment.

While the mass-gain term, s, can represent any mass gain or loss, the most likely application to jets is entrainment or mass pickup from the surroundings. In this application, s will be in general a function of time and space, as entrainment occurs at the head of a propagating jet as well as along its sides (see the simulations of De Young 1986; or the more detailed treatment of Bicknell 1986c). However more heuristic treatments are possible (e.g., De Young 1981) and may prove to be useful in looking for simple analytic approaches.

Analyses of jet bending in the literature assume $\boldsymbol{F}_{\rm ext}$ and $s\boldsymbol{v}$ are small, and that $\nabla p_{\rm ext}$ is applied transverse to the beam (e.g., Jones & Owen 1979; Eilek et al. 1984; O'Dea 1984). The velocity is taken to change by its own magnitude over the bending scale, $l_{\rm bend}$. Alternatively, the system can be described in terms of a pressure gradient that provides the centripetal acceleration $v^2/l_{\rm bend}$ around a curve of radius $l_{\rm bend}$. Writing v_b and ρ_b as the velocity and density at the bend, both of these approaches yield

$$\rho b \frac{v_b^2}{l_{\rm bend}} = -\nabla p_{\rm ext} . \tag{A9}$$

Further, for a beam deflected by the ram pressure of an impinging ICM due to the motion of the galaxy, we can write $\nabla p_{\rm ext} \simeq \rho_{\rm ICM} v_g^2/l_{\rm pressure}$, where v_g is the velocity of the galaxy with respect to the ICM and $l_{\rm pressure}$ is the length scale over which the pressure gradient acts. Thus, equation (A9) becomes

$$\rho b \frac{v_b^2}{l_{\rm bend}} = \rho_{\rm ICM} \frac{v_g^2}{l_{\rm pressure}} , \tag{A10}$$

which is the equation from which the analysis of radio source bending proceeds.

APPENDIX B

SURFACE BRIGHTNESS OF ADIABATIC FLOWS

If the electrons in the flow suffer only adiabatic losses, and if the magnetic field obeys flux freezing, the surface brightness of the flow can be predicted. We follow Fanti et al. (1982) and Owen et al. (1985); Perley, Bridle, & Wills (1984) and also Bicknell (1984) have developed similar approaches.

For a power-law distribution of energies, the number of electrons with energies between E and $E + dE$ is given by

$$N(E)dE = N_o E^{-\gamma s} dE , \tag{B1}$$

where N_o is a scale factor and γ_s is the electron energy spectral index. This power law must have a low-energy cutoff, $E_{\rm min}$. The volume emissivity is

$$\epsilon_\nu = c_5(\gamma_S) N_o (B \sin \vartheta)^{1/2(\gamma s+1)} \left(\frac{\nu}{2c_1}\right)^{1/2(1-\gamma s)} \tag{B2}$$

where ϑ is the angle between the magnetic field and the line of sight and the constants are given by Pacholczyk (1970).

The luminosity behavior down the tail, taking into account the adiabatic expansion, is of concern here. To examine the dependence of the emissivity on the magnetic field, we note that the essential dependence of equation (B1) is, $\epsilon_\nu \propto N_o B^{1/2(\gamma s+1)}$. In an adiabatically expanding jet or tail where magnetic flux is conserved, the evolution of dominantly parallel and perpendicular fields differ and are given by

$$B_\parallel \propto \frac{1}{r^2} , \quad B_\perp \propto \frac{1}{rv} , \tag{B3}$$

where r is the radius and v the velocity of the beam. The difference is based in the difference in the evolution of sample areas oriented perpendicular (for $B_\parallel$) and parallel (for $B_\perp$) to the beam. The area of the first goes simply as the area of the beam, whereas the area of the second depends upon the width of the beam (r) and the changing of the length due to the changing velocity (the length of the sample area is some $l = vt$ for a standard sample time t). For a power-law distribution of relativistic particles, the total number density (over all energies) is given by

$$n_{\rm rel} = \int_{E_{\rm min}}^{\infty} N(E)dE = \frac{1}{\gamma_S - 1} N_o E_{\rm min}^{1-\gamma s}$$

Thus, the coefficient

$$N_o \propto n_{\rm rel} E_{\rm min}^{\gamma s - 1} \tag{B4}$$

will change with the total number density and the energy. Adiabatic volume changes affect the pressure as $p_{\rm rel} \propto n_{\rm rel}^{4/3}$, where we have used $\gamma_A = 4/3$ for relativistic particles. The mean energy per particle, $e_{\rm rel} = 3p_{\rm rel}/n_{\rm rel}$; but also $e_{\rm rel} = n_{\rm rel}^{-1} \int_{E_{\rm min}}^{\infty} EN(E)dE \propto E$. Thus, $E_{\rm min} \propto n_{\rm rel}^{1/3}$. Now, conserving the number flux of relativistic particles in the beam, we have $n_{\rm rel} \propto 1/r^2 v$, which gives

$$N_o \propto n_{\rm rel}^{1/3(\gamma s+2)} \propto (r^2 v)^{-1/3(\gamma s+2)} . \tag{B5}$$

Using equations (B3) and (B5) in (B2) gives, for the two magnetic field geometries, expressions for the volume emissivity:

$$\epsilon_\parallel \propto v^{-1/3(\gamma s+2)} r^{-1/3(5\gamma s+7)} , \tag{B6}$$

$$\epsilon_\perp \propto v^{-1/6(5\gamma s+7)} r^{-1/6(7\gamma s+11)} . \tag{B7}$$

For a circular flow, the cross-sectional area is proportional to the radius squared, and the luminosity per unit length is given by $\mathscr{L}_\nu \propto \varepsilon_\nu r^2$. Thus, we end up with

$$\mathscr{L}_{\nu\parallel} \propto \nu^{-1/3(\gamma_S+2)_r-1/3(5\gamma_S+1)}, \tag{B8}$$

$$\mathscr{L}_{\nu\perp} \propto \nu^{-1/6(5\gamma_S+7)_r-1/6(7\gamma_S-1)}. \tag{B9}$$

which are the expressions used in the text.

APPENDIX C

SPECTRAL STEEPENING

An electron of energy E, and pitch angle ϑ, loses energy in a magnetic field, B, at a rate

$$\frac{dE}{dt} = -c_2 B^2 E^2 \sin^2 \vartheta \tag{C1}$$

where $c_2 = 2e^4/3m_e^4 c^7 = 2.37 \times 10^{-3}$ in cgs units. An electron energy spectrum which is initially a power law, given in equation (B1), after a time t will steepen at energies $\gtrsim E_{\rm break}$ where $E_{\rm break}$ is given by

$$c_2 E_{\rm break} \int_0^t B^2(\tau) d\tau \gtrsim 1 \tag{C2}$$

(e.g., van der Laan & Perola 1969 or Pacholczyk 1970). We have extended this formula to allow the magnetic field the electron sees to vary with time (e.g., Eilek & Shore 1989). [We also note that $B^2(\tau)$ must include both the true local magnetic field, and the squared Compton equivalent field, B_c^2, in order to account for all losses].

The break in the electron spectrum produces a break in the radiated photon spectrum,

$$\nu_{\rm break}(t) = c_1 E_{\rm break}^2 B(t), \tag{C3}$$

where $c_1 = e3/4\pi m_e^3 c^5 = 6.27 \times 10^{18}$ in cgs units. We note that $\nu_{\rm break}$ depends on the instantaneous, not rms (time-averaged) magnetic field. Combining equations (C2) and (C3), and writing $B_{\rm rms}^2 = t^{-1} \int_0^t B^2(\tau) d\tau$, we have

$$\nu_{\rm break} = \frac{c_1}{c_2^2} \frac{B(t)}{(B_{\rm rms}^2 + B_c^2)^2 t^2}. \tag{C4}$$

Putting in the numerical constants, and scaling $\nu_{\rm break}$ to the rest frame of a source at redshift z_R, we can express this implicitly in terms of the elapsed time, t (Myers & Spangler 1985; Alexander 1986):

$$t = 3.35 \times 10^4 \frac{B^{1/2}(t)}{B_{\rm rms}^2 + B_c^2} \frac{1}{[(1+z_R)\nu_{\rm break}]^{1/2}} \text{ yr} \tag{C5}$$

where B is in Gauss and $\nu_{\rm break}$ in Hz.

In order to derive the age of plasma at a point z down the tail, we want to find $\nu_{\rm break}$ from the 6 and 20 cm spectral index. As in Myers & Spangler, the frequency dependence of the synchrotron emissivity at a given ν depends on the integral of the single-particle power over the electron distribution:

$$\epsilon(\nu, t) = 4\pi c_3 B \sin \vartheta \int_0^{E_{\rm break}} F(X) N(E, \vartheta, t) dE. \tag{C6}$$

Here, the function $F(X)$ is given by

$$F(X) = X \int_X^\infty K_{5/3}(q) dq \tag{C7}$$

and $X = \nu/\nu_{\rm break}$. Following Jaffe & Perola (1973), and Alexander (1986), we assume the particles are well scattered in pitch angle, so that the radiative losses are governed by a single, mean pitch angle. If the particle distribution is initially isotropic, and the particles do not scatter in pitch angle, then the integral in equation (C6) must be taken over ϑ as well.

If the electron distribution started as in equation (B1) at $t = 0$, at time t it has the form

$$N(E, \vartheta, t) = N_o E^{-\gamma_S} (1 - c_2 E B_{\rm rms}^2 \sin^2 \vartheta t)^{\gamma_S - 2} \tag{C8}$$

(van der Laan & Perola 1969; Pacholczyk 1970). Clearly, insertion of equations (C7) and (C8) in equation (C6) does not produce an analytic expression for the frequency dependence of $\epsilon(\nu)$. The integral in equation (C6) was done analytically by Alexander (1986), who tabulated the spectral index at 20 cm as a function of X, for three values of γ_S (we reproduce his values in Fig. 4). We use his results to find $\nu_{\rm break}(z)$, and hence $t(z)$ from (C5), from the 6 and 20 cm spectra for our sources.

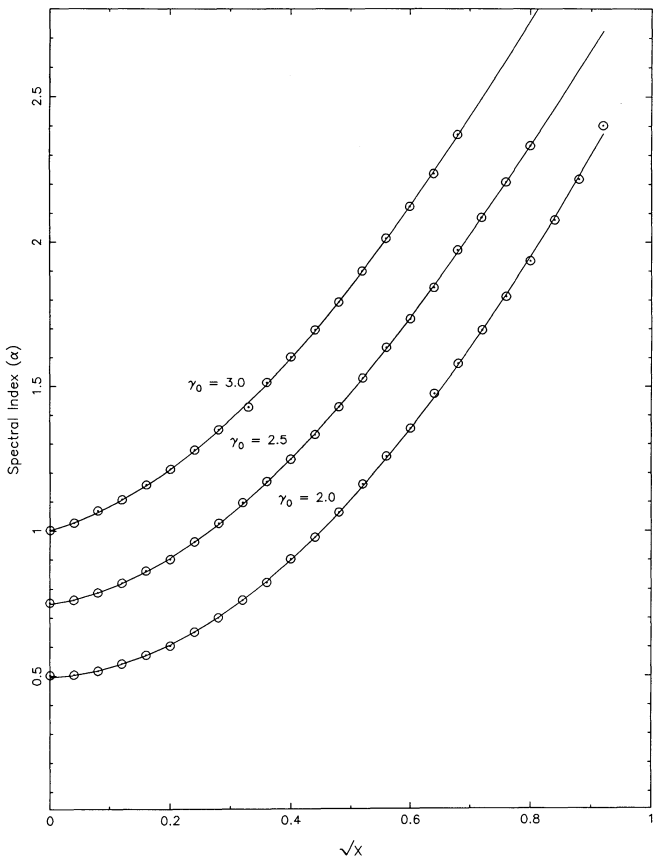

FIG. 4.—The photon spectral index, α, as a function of the X parameter, for three values of the initial particle spectral index, γ_o. Taken from Alexander (1986).

REFERENCES

Abell, G. O. 1958, ApJS, 3, 211
Alexander, P. 1986, Ph.D. thesis, Cambridge Univ.
Bateman, G. 1978, MHD Instabilities (Cambridge: MIT Press)
Bautz, L. P. 1972, AJ, 77, 1
Bautz, L. P., & Morgan, W. W. 1970, ApJ, 162, L149
Benford, G. 1978, MNRAS, 183, 29
Bicknell, G. V. 1984, ApJ, 286, 68
———. 1986a, Canadian J. Phys., 64, 495
———. 1986b, ApJ, 300, 591
———. 1986c, ApJ, 305, 109
Bicknell, G. V., & Melrose, D. B. 1982, ApJ, 262, 511
Bicknell, G. V., de Ruiter, H. R., Cameron, R. A., & Gingold, R. A. 1990, ApJ, 354, 98
Borovsky, J. O. 1986, ApJ, 306, 451
Bridle, A. H., & Perley, R. A. 1984, ARA&A, 22, 319
Burns, J. O. 1981, MNRAS, 195, 523
Burns, J. O., & Balonek, T. 1982, ApJ, 263, 546
Burns, J. O., Owen, F. N., & Rudnick, L. 1979, AJ, 84, 1683
Caganoff, S., Bicknell, G. V., & Carter, D. 1985, Proc. Astron. Soc. Australia, 6, 151
Carilli, C. 1989, Ph.D. thesis, Massachusetts Institute of Technology
De Young, D. S. 1981, Nature, 293, 43
———. 1986, ApJ, 307, 62
———. 1990, ApJ, 371, 69
Eilek, J. A. 1979, ApJ, 230, 373
———. 1984, in IAU Symp. 107, Unstable Current Systems and Plasma Instabilities in Astrophysics, ed. M. Kundu (Reidel: Boston), 433
Eilek, J. A., Burns, J. O., O'Dea, C. P., & Owen, F. N. 1984, ApJ, 278, 37
Eilek, J. A., & Shore, S. S. 1989, ApJ, 342, 187
Fanaroff, B. L., & Riley, J. M. 1974, MNRAS, 167, 31P
Fanti, R., Lari, C., Parma, D., Bridle, A. H., Ekers, R. D., & Fomalont, E. B. 1982, A&A, 110, 169
Feretti, L., Giovannini, G., Gregorini, L., Padrielli, L., Roland, J., & Valenijn, E. A. 1985, A&A, 147, 321
Feretti, L., Spazzoli, O., Gioia, I. M., Goivannini, G., & Gregorini, L. 1990, A&A, 233, 325
Ge, J.-P. 1991, Ph.D. thesis, New Mexico Institute of Mining and Technology
Hill, J. M., Hintzen, P., Oegerle, W. R., Romanishin, W., Lesser, M. P., Eisenhamer, J. D., & Batuski, D. J. 1988, ApJ, 332, L23
Hines, D. C., Owen, F. N., & Eilek, J. A. 1989, ApJ, 347, 713
Hu, E. M., Cowie, L. L., & Wang, Z. 1985, ApJS, 59, 447
Jaffe, W. J., & Perola, G. C. 1973, A&A, 26, 423
Jones, C., & Forman, W. 1984, ApJ, 276, 38
Jones, T. V., & Owen, F. N. 1979, ApJ, 234, 818
Laing, R. 1981, ApJ, 248, 887
Landau, L. D., & Lifshitz, E. M. 1959, Fluid Mechanics (New York: Pergamon)
Leahy, J. P. 1984, MNRAS, 208, 323
Leir, A. A., & van den Bergh, S. 1977, ApJS, 34, 381
Malumuth, E. 1989, in Clusters of Galaxies, ed. M. J. Fichett & W. R. Oegerle (Baltimore Space Telescope Science Institute), 157
Mathews, W. G., & Baker, J. C. 1971, ApJ, 170, 241
McHardy, I. M. 1974, MNRAS, 169, 527
Myers, S. T., & Spangler, S. R. 1985, ApJ, 291, 52
Norman, M. L., Smarr, L., Winkler, K.-H. A., & Smith, M. D. 1982, A&A, 113, 285
Norman, M. L., Burns, J. O., & Sulkanen, M. 1988, Nature, 335, 146
O'Dea, C. P. 1984, Ph.D. thesis, University of Massachusetts
O'Dea, C. P., & Baum, S. 1986, in Proc. NRAO Workshop 16, Radio Continuum Processes in Clusters of Galaxies, ed. C. P. O'Dea & J. M. Uson (Green Bank, WV: NRAO), 141
O'Donoghue, A. A. 1989, Ph.D. thesis, New Mexico Tech
O'Donoghue, A. A., Owen, F. N., & Eilek, J. A. 1990, ApJS, 72, 75 (O^2E)
Owen, F. N. 1975, AJ, 80, 263
Owen, F. N., Eilek, J. A., & Keel, W. C. 1993, in preparation
Owen, F. N., Hardee, P. E., & Cornwell, T. J. 1988, ApJ, 340, 698
Owen, F. N., & Laing, R. A. 1989, MNRAS, 238, 357
Owen, F. N., O'Dea, C. P., Inoue, M., & Eilek, J. A. 1985, ApJ, 294, L85
Owen, F. N., O'Dea, C. P., & Keel, W. C. 1990, ApJ, 352, 44
Owen, F. N., & Rudnick, L. 1976, ApJ, 205, L1
Owen, F. N., & White, R. A. 1991, MNRAS, 249, 164
Owen, F. N., White, R. A., & Burns, J. O. 1991, preprint

Owen, F. N., White, R. A., Hilldrup, K. C., & Hanisch, R. J. 1982, AJ, 87, 1083
Owen, F. N., White, R. A., & Thronson, H. A. 1988, AJ, 95, 1
Pacholczyk, A. G. 1970, Radio Astrophysics (San Francisco: Freeman)
Patnaik, A. R., Banhatti, D. G., & Subranhmanya, C. R. 1984, MNRAS, 211, 775
Patnaik, A. R., Malkan, M. A., & Salter, C. J. 1986, MNRAS, 220, 351
Perley, R. A., Bridle, A. H., & Wills, A. G. 1984, ApJS, 54, 291
Quintana, H., & Lawrie, D. G. 1982, AJ, 87, 1
Roland, J., Veron, J., Paulini-Toth, I. I. K., Preuss, E., & Witzel, A. 1975, A&A, 50, 165
Rudnick, L., & Owen, F. N. 1977, AJ, 82, 1
Sharpels, R. M., Ellis, R. S., & Gray, P. M. 1988, MNRAS, 231, 479
Simon, A. J. B. 1978, ApJ, 23, 113
van Breugel, W. J. M. 1980, A&A, 88, 248
van der Laan, H., & Perola, G. C. 1969, A&A, 3, 468
Wentzel, D. G. 1974, ARA&A, 12, 71
Zhao, J.-H. 1990, Ph.D. thesis, University of New Mexico